

# Electronic transport through a graphene-based ferromagnetic/normal/ferromagnetic junction

Jiang-chai Chen<sup>1</sup>, Shu-guang Cheng<sup>2</sup>, Shun-Qing Shen<sup>3</sup>, and Qing-feng Sun<sup>1,\*</sup>

<sup>1</sup>Beijing National Lab for Condensed Matter Physics and Institute of Physics, Chinese Academy of Sciences, Beijing 100190, China

<sup>2</sup>Department of Physics, Northwest University, Xi'an 710069, China

<sup>3</sup>Department of Physics, and Center of Theoretical and Computational Physics, The University of Hong Kong, Hong Kong, China

E-mail: sunqf@aphy.iphy.ac.cn

**Abstract.** Electronic transport in a graphene-based ferromagnetic/normal/ferromagnetic junction is investigated by means of Landauer-Büttiker formalism and the nonequilibrium Green's function technique. For the zigzag edge case, the results show that the conductance is always larger than  $e^2/h$  for the parallel configuration of lead magnetizations, but for the antiparallel configuration the conductance becomes zero because of the band-selective rule. So a magnetoresistance (MR) plateau emerges with the value 100% when the Fermi energy is located around the Dirac point. Besides, choosing narrower graphene ribbons can obtain the wider 100% MR plateaus and the length change of the central graphene region does not affect the 100% MR plateaus. Although the disorder will reduce the MR plateau, the plateau value can be still kept about 50% even in a large disorder strength case. In addition, when the magnetizations of the left and right leads have a relative angle, the conductance changes as a cosine function of the angle. What is more, for the armchair edge case, the MR is usually small. So, it is more favorable to fabricate the graphene-based spin valve device by using the zigzag edge graphene ribbon.

## 1. Introduction

Graphene, a two-dimensional single-layer crystal of carbon atoms arraying in a honeycomb lattice, is a novel and exciting material [1]. The low energy excitation of a graphene has a linear dispersion relation, and the dynamics of the charge carriers obeys the massless Dirac-like equation [2]. Because of the unique band structures, the graphene has many peculiar properties, such as that the Hall plateaus occur at half-integer multiples of  $ge^2/h$  with the spin and valley degeneracy  $g = 4$ , and the conductivity at the zero magnetic field has a non-zero minimal value [3]. For the neutral graphene, its Fermi level is located at the Dirac points, the corners of the hexagonal first Brillouin zone. In experiment, a gate voltage can be used to tune the Fermi level, which can be above or below the Dirac points [4]. In addition, graphene also exhibits many excellent transport characteristics: the high mobility [5], long spin relaxation length [6], and stable behaviors under ambient conditions. At room temperature, its mobilities can be above  $10^4 \text{cm}^2/\text{V} \cdot \text{s}$ , implying that the mean free path can be as long as a few hundred nanometers. Because of weak spin-orbit coupling [7] and low hyperfine interaction [8], its spin relaxation length can reach the order of the micrometer at room temperature. Thus, graphene may be an excellent candidate for microelectronic applications, in particular for spintronic applications [9].

In general, the charge carriers in graphene are not spin-polarized. For spintronic applications, people try to inject the spin-polarized current or to induce the spin-polarized carriers in the graphene. Recently, many works are focusing on this issue. For example, Haugen *et al* [10] suggested that the spin-polarized carriers can be realized by growing the graphene on a ferromagnetic (FM) insulator (e.g. EuO). Owing to the magnetic proximity effect, an exchange split between the spin-up and spin-down carriers in the graphene is induced, and then the carriers are spin-polarized. Based on the first-principles calculations, Son *et al* [11] predicted that the zigzag graphene nanoribbon becomes a half metal when an in-plane transverse electric field is applied. Also, Lin *et al* [12] demonstrated that electron-electron correlation in armchair graphene nanoribbon can generate the flat-band ferromagnetism. On the experiment side, a large spin injection into the graphene has been realized by connecting the graphene to an FM electrode [6, 13, 14]. Furthermore, several groups [14, 15] have performed nonlocal magnetoresistance(MR) measurements, in which a net spin current is brought between the injector and detector.

The well-known application in spintronics is the spin-valve effect [16], in which the resistance of devices can be changed by manipulating the relative orientation of the magnetizations. Motivated by the spintronic application with the novel material, the spin-polarized transport through graphene are currently attracting a great deal of attentions [17, 18, 19, 20, 21, 22, 23]. Using the tight-binding model, Brey and Fertig [20] studied the MR of the FM/graphene/FM junction in the limit of infinite width. They found that the MR is rather small since the conductivity is weakly dependent on the relative magnetization orientations of FM leads. Ding *et al* [21] investigated the

similar device with two FM leads by a continuous model. The results showed that the MR versus the bias exhibits a cusp around the zero bias in absence of external magnetic field and oscillating behavior at the high magnetic field. Based on the first-principles calculation, Kim and Kim [22] predicted that a graphene-based spin-valve device could have a high MR.

In this paper, we study the conductance and MR of a graphene-based spin valve. The device consists of a graphene nanoribbon coupling to two FM leads, as shown in figure 1(a). Here the width of the device is finite in the order of 10 nanometers, i.e. the size effect is considered. In recent experiments [24], a few 10-nanometer or sub-10-nanometer graphene nanoribbons have already been fabricated successfully. For a finite-width graphene nanoribbon, the wave vectors along the confined direction are discrete, and the transverse subbands emerge. The characteristics of the subbands are strongly dependent on the chirality of the graphene-nanoribbon edge [25], e.g. the zigzag edge or armchair edge. So the conductance and MR should be strongly dependent on the boundary condition of graphene nanoribbon. In addition, we consider that two FM leads also have the hexagonal lattice structure as the graphene. In other words, the leads are graphene-based FM or called the FM graphene. On the experiment, the FM electrode (e.g. the cobalt electrode) usually overlaps on the graphene through a thin oxide layer [6, 14]. Because of the magnetic proximity effect and the Zeeman effect, an exchange split in the graphene underneath the oxide layer is induced, then its carriers are spin-polarized. So the graphene covered with the FM electrode has the magnetization. Then the spin-polarized charge carriers, driven by a bias, travel from one FM graphene through the central normal graphene to another FM graphene.

In the tight-binding model the Landauer-Büttiker formula and non-equilibrium Green's function method are applied to calculate the conductance and MR. For the zigzag graphene ribbon case, we found that when the graphene nanoribbon is narrow enough and its separation  $\Delta$  between the first subband and the zeroth subband is larger than the exchange split energy  $M$ , the conductance for the antiparallel magnetization configuration can almost be zero in a quite large energy window around the Dirac point. But for the parallel configuration the conductance is always larger than  $e^2/h$ , so the MR exhibits a plateau with the value 100%. As the width of the nanoribbon increases, the sub-band separation  $\Delta$  gradually decreases, and the MR can keep at the value 100% at the beginning of  $\Delta > M$ , then decreases when  $\Delta < M$ . In the presence of the disorder, the MR slightly drops, but even in quite large disorder it can keep the value 50%, which is still much larger than 10%, the lower limit of the giant magnetoresistance effect. What is more, for the armchair graphene nanoribbon case, the MR is always small regardless of the width of nanoribbon. By comparing two cases of graphene ribbons with different edges, it is more reasonable to apply zigzag graphene ribbons to the spin-valve devices.

The rest of the paper is organized as follows: In Section 2, we describe the model and the details of the calculations. In Sections 3 and 4 we will give the numerical results of the conductance and MR for the zigzag and armchair edge cases, respectively. Finally, a brief conclusion is presented in Section 5.

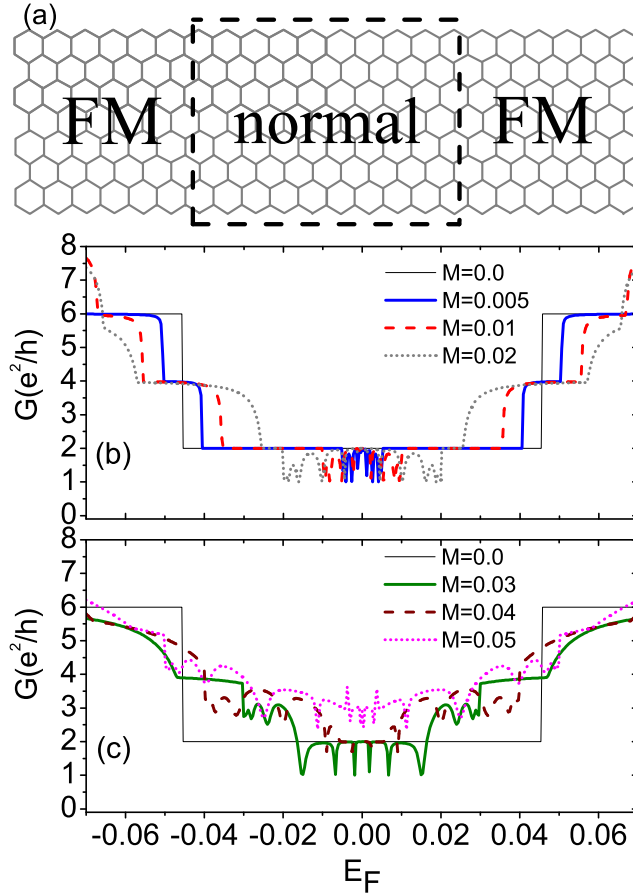


**Figure 1.** (Color online)(a).The schematic of a graphene-based FM/normal/FM junction. (b) and (c): the conductance  $G$  vs. the Fermi energy  $E_F$  for the different magnetization  $M$  at the parallel configuration ( $\theta = 0$ ). The size of the central graphene is  $N = 50$  and  $L = 10$ .

## 2. Model and formulations

We consider a graphene-based spin valve (as shown in figure 1(a)) which consists of a central normal graphene strip and two FM graphene ribbons. The total Hamiltonian  $H$  of the device can be divided into four terms,  $H = H_C + H_L + H_R + H_T$ , where  $H_C$  describes the central normal graphene region,  $H_L$  and  $H_R$  are the Hamiltonian of the left and right FM-graphene leads, respectively, and  $H_T = H_{TL} + H_{TR}$  is the coupling Hamiltonian of central region to the left and right leads. In the tight-binding approximation[26], the Hamiltonians  $H_C$ ,  $H_L$ ,  $H_R$ , and  $H_T$  can be written as

$$\begin{aligned}
 H_C &= \sum_{i \in C} \epsilon_C a_i^\dagger \sigma_I a_i - \sum_{\langle ij \rangle (i,j \in C)} (t a_i^\dagger \sigma_I a_j + h.c.), \\
 H_{\alpha=L,R} &= \sum_{i \in \alpha} a_i^\dagger (\epsilon_\alpha \sigma_I + \boldsymbol{\sigma} \cdot \mathbf{M}_\alpha) a_i \\
 &\quad - \sum_{\langle ij \rangle (i,j \in \alpha)} (t a_i^\dagger \sigma_I a_j + h.c.),
 \end{aligned}$$

$$H_T = - \sum_{\langle ij \rangle (i \in C, j \in L, R)} (t a_i^\dagger \sigma_I a_j + h.c.),$$

where  $s = \uparrow, \downarrow$  represents the spin of electrons;  $a_{is}^\dagger$  ( $a_{is}$ ) creates (annihilates) an electron with spin  $s$  on site  $i$ , and  $a_i = \begin{pmatrix} a_{i\uparrow} \\ a_{i\downarrow} \end{pmatrix}$ ;  $\langle ij \rangle$  stands for a nearest-neighbor pair.  $\boldsymbol{\sigma} = (\sigma_x, \sigma_y, \sigma_z)$  are the Pauli matrices and  $\sigma_I$  is a  $2 \times 2$  unit matrix.  $\epsilon_C$ ,  $\epsilon_L$ , and  $\epsilon_R$  are the on-site energies (i.e. the energy of the Dirac point) in the center region, left and right FM leads, respectively, which can be tuned by the gate voltage. The size of the center graphene region is described by the width  $N$  and length  $L$ . In figure 1(a), a zigzag edge graphene nanoribbon with  $N = 4$  and  $L = 9$  is shown. The terms including the factor  $t$  in Hamiltonian describe the nearest neighbor hopping with the hopping energy  $t$ .  $\mathbf{M}_L$  and  $\mathbf{M}_R$  are the magnetizations of the left and right FM leads. Here we allow that the magnetizations  $\mathbf{M}_L$  and  $\mathbf{M}_R$  can be along arbitrary direction. Without loss of generality we assume that the magnetization  $\mathbf{M}_L$  of left lead is along the z-axis, then  $\mathbf{M}_L = M_L(0, 0, 1)$ , and the magnetization  $\mathbf{M}_R$  of the right lead is along the direction  $(\theta, \varphi)$  with  $\mathbf{M}_R = M_R(\sin \theta \cos \varphi, \sin \theta \sin \varphi, \cos \theta)$ .

Before performing the calculation, we take a unitary transformation with  $\tilde{a}_i = U a_i$  for all site  $i$  in the right FM lead, where the unitary matrix  $U$  is

$$U = \begin{pmatrix} \cos(\theta/2) & e^{-i\varphi} \sin(\theta/2) \\ e^{i\varphi} \sin(\theta/2) & -\cos(\theta/2) \end{pmatrix}.$$

Under this unitary transformation, the Hamiltonians  $H_C$ ,  $H_L$ , and  $H_{TL}$  remain unchanged, and  $H_R$  and  $H_{TR}$  vary into

$$\begin{aligned} H_R &= \sum_{i \in R} \tilde{a}_i^\dagger (\epsilon_R \sigma_I + \boldsymbol{\sigma} \cdot \mathbf{M}'_R) \tilde{a}_i \\ &\quad - \sum_{\langle ij \rangle (i, j \in R)} (t \tilde{a}_i^\dagger \sigma_I \tilde{a}_j + h.c.), \\ H_{TR} &= - \sum_{\langle ij \rangle (i \in C, j \in R)} (t a_i^\dagger U \tilde{a}_j + h.c.), \end{aligned}$$

where  $\mathbf{M}'_R = M_R(0, 0, 1)$ . After the unitary transformation, the z-axis of the spin in the right FM lead is along the direction of  $\mathbf{M}'_R$ , and the Hamiltonian  $H_R$  is diagonal in the spin space.

The current flowing through the device can be calculated from the Landauer-Büttiker formula [27]

$$I = (e/h) \int d\epsilon T_{LR}(\epsilon) [f_L(\epsilon) - f_R(\epsilon)],$$

where  $f_{L/R}(\epsilon) = 1/\{exp[(\epsilon - \mu_{L/R})/k_B T] + 1\}$  is the Dirac-Fermi distribution function of the left and right FM leads and  $T_{LR}(\epsilon) = \text{Tr}[\boldsymbol{\Gamma}_L \mathbf{G}^r \boldsymbol{\Gamma}_R \mathbf{G}^a]$  is the transmission coefficient, with the line-width function  $\boldsymbol{\Gamma}_\alpha(\epsilon) = i[\boldsymbol{\Sigma}_\alpha^r(\epsilon) - \boldsymbol{\Sigma}_\alpha^a(\epsilon)]$  and the Green's functions  $\mathbf{G}^r(\epsilon) = [\mathbf{G}^a(\epsilon)]^\dagger = \mathbf{1}/[\epsilon - \mathbf{H}_C - \boldsymbol{\Sigma}_L^r - \boldsymbol{\Sigma}_R^r]$ .  $\boldsymbol{\Sigma}_{L/R}^r$  is the retarded self-energy function coupling to the leads, which has to be calculated numerically by solving the surface Green's function of the leads [28, 29]. After solving the current  $I$ , the linear conductance  $G$  can be obtained straightforwardly,  $G = \lim_{V \rightarrow 0} dI/dV$ , with the bias

$V = \mu_L - \mu_R$ . At zero temperature  $G = (e^2/h)T(E_F)$ . In the numerical calculation, we take the nearest-neighbor hopping energy  $t = 1$  as the energy unit and adopt the Dirac point energies  $\epsilon_L = \epsilon_R = \epsilon_C = 0$ . The magnetizations  $M_\alpha$  in the left and right FM leads are assumed to be equal ( $M_L = M_R = M$ ), which is usually reasonable when two FM leads are made of the same material. The angle  $\varphi = 0$  because the conductance and MR are independent of  $\varphi$ .

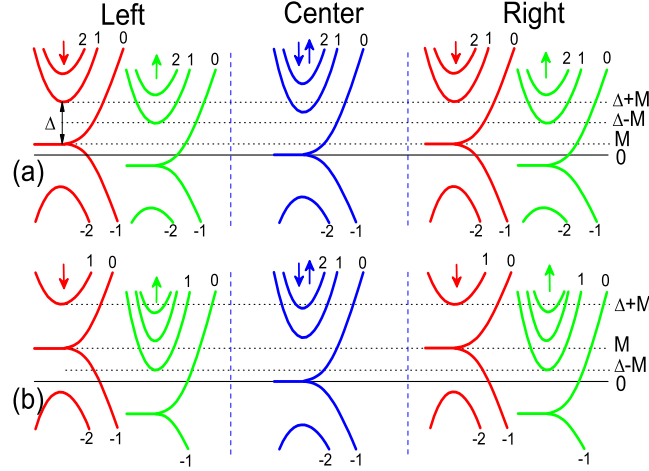


**Figure 2.** (Color online) The energy band structures of the left lead, center region, and right lead in the case of the zigzag edge at the parallel configuration ( $\theta = 0$ ). (a)  $0 < M < \Delta/2$  and (b)  $\Delta/2 < M < \Delta$ .

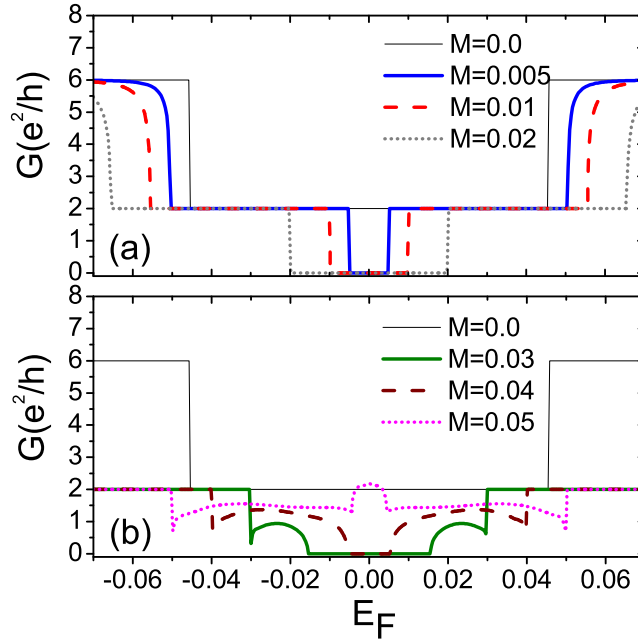


**Figure 3.** (Color online) The conductance  $G$  vs. the Fermi energy  $E_F$  for the different  $M$  at the antiparallel configuration ( $\theta = \pi$ ). The size of system is the same as figure 1(b).

### 3. The case of zigzag edge

In this section, we focus on the zigzag edge graphene-based spin valves. We first investigate the conductance  $G$  on the parallel and antiparallel configurations, and then the MR and the conductance on the arbitrary angle between magnetizations  $\mathbf{M}_L$  and  $\mathbf{M}_R$ .

#### 3.1. The conductance for the parallel configuration

Figures 1(b) and (c) show the conductance  $G$  versus the Fermi energy  $E_F$  for different magnetization  $M$  of the parallel configuration (i.e.  $\theta = 0$ ). When the magnetization  $M = 0$ , the two leads are normal and the whole device is a flawless graphene ribbon. In this case, the conductance  $G$  exhibits the plateau structure with the plateau values at  $2, 6, 10, \dots$  (in the unit  $e^2/h$ ), i.e. at the half-integer position,  $g(n + 1/2)e^2/h$  with the degeneracy  $g = 4$ , due to the transverse sub-band structures. The step height of the value  $4e^2/h$  results from spin and valley degeneracy and the plateaus at half-integer value originates from the fact that the zeroth subband has the only spin degeneracy.

When the two leads are FM with a non-zero  $M$ , the conductance  $G$  does not have the perfect plateau structure, but still obeys the electron-hole symmetry,  $G(-E_F) = G(E_F)$  (see figures 1(b) and (c)). In the following, we discuss the conductance  $G$  in details for  $0 < M < \Delta/2$  and  $\Delta/2 < M < \Delta$ , where  $\Delta$  is the energy splitting between the first subband and the zeroth subband (see figure 2) and  $\Delta \approx 0.045$  for  $N = 50$ . For  $0 < M < \Delta/2$ , the curve of  $G$  versus  $E_F$  can be partitioned into several regions:  $(0, M)$ ,  $(M, \Delta - M)$ ,  $(\Delta - M, \Delta + M)$ , etc. In the first interval of  $E_F \in (0, M)$ , the conductance  $G$  oscillates with the value between  $e^2/h$  and  $2e^2/h$ . In the interval of  $E_F \in (M, \Delta - M)$ , the conductance  $G$  is exactly equal to  $2e^2/h$  and forms a plateau. In the interval of  $E_F \in (\Delta - M, \Delta + M)$ , the conductance approaches the value  $4e^2/h$ . With the rising of  $E_F$  further, the conductance becomes larger.

In order to understand above results, we present the energy bands of the left lead, center region, and right lead in figure 2, and the band index is specified in each region. Owing to the symmetry of bands, only the part of the moment  $k > 0$  is shown. The 0-th and  $-1$ -th subbands in the FM leads are nondegenerate, but other subbands are two-fold degenerated. Because of the parity conservation of the transverse wave function, the electrons belonging to the even (odd) parity subbands in the left FM lead are transported only into the even (odd) parity subbands of the right lead, which was demonstrated in a very recent letter [30] and it is named the band-selective phenomenon. For convenience, we use the symbol  $(i, j, k)$  to denote the channel through which electrons are transported from the  $i$ -th band of the left lead, through the  $j$ -th band in the center region, to the  $k$ -th band of the right lead, and  $T_{i,j,k}$  to denote its transmission coefficient.

With the aid of energy bands in figure 2(a), we now explain the conductance  $G$  in figure 1(b) with  $0 < M < \Delta/2$ . (i) When  $E_F \in (0, M)$ , the channel  $(0, 0, 0)$  is open for spin-up electrons, and  $T_{0,0,0}$  is exactly 1 due to lack of the scattering. For spin-down electrons, the channel  $(-1, 0, -1)$  is open, in which the parity of the transverse wave

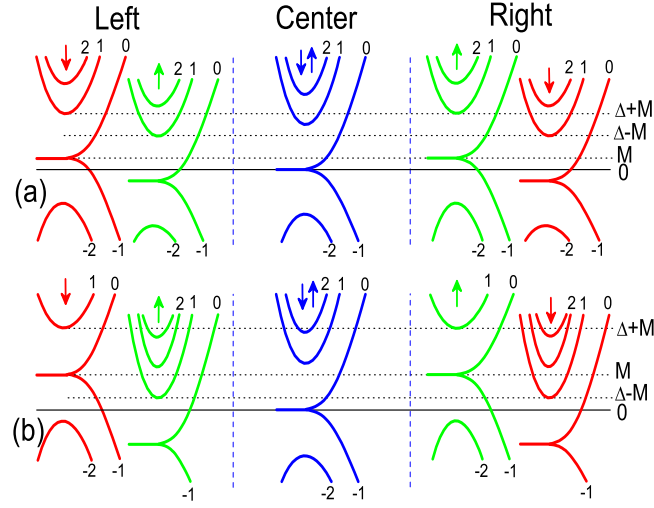


**Figure 4.** (Color online) The energy band structures of the left lead, center region, and right lead for the zigzag edge case at the antiparallel configuration ( $\theta = \pi$ ). **(a)**  $0 < M < \Delta/2$  and **(b)**  $\Delta/2 < M < \Delta$ .

function in the center region mismatches with that of the left and right lead, so the scattering exists and  $0 < T_{-1,0,-1} < 1$ . As a result, total conductance oscillates with its value between  $e^2/h$  and  $2e^2/h$ . (ii) When  $E_F \in (M, \Delta - M)$ , the channels  $(0, 0, 0)$  are available for both the spin-up and spin-down electrons, and the conductance  $G$  exactly equals to  $2e^2/h$ . (iii) Furthermore,  $E_F$  increases to the range of  $(\Delta - M, \Delta + M)$ . Besides the channels  $(0, 0, 0)$  of both spin electrons, the channels  $(1, j, 1)$  ( $j = 0, 1$ ) of the spin-up take part in the transport, which make the conductance  $G$  approximate  $4e^2/h$ .

Now we discuss the conductance in the case of  $\Delta/2 < M < \Delta$ . Figure 1(c) shows the conductance, and the corresponding band structure is shown in figure 2(b). Apparently, the conductance  $G$  varies more complex than that in  $0 < M < \Delta/2$  (see figures 1(b) and (c)). Here we are mainly concerned about two energy regions:  $E_F \in (0, \Delta - M)$  and  $(\Delta - M, M)$ . When  $E_F \in (0, \Delta - M)$  the transport involves the channel  $(0, 0, 0)$  of spin-up electrons and the channel  $(-1, 0, -1)$  of spin-down electrons. So the conductance  $G$  oscillates between  $e^2/h$  and  $2e^2/h$ , which is identical with case (i) when  $0 < M < \Delta/2$ . For  $E_F \in (\Delta - M, M)$ , another channel  $(1, 0, 1)$  of spin-up electrons joins into the transport, so the conductance is obviously enhanced and the value lies between  $2e^2/h$  and  $4e^2/h$ . Further, for  $E_F > M$ , because more channels will be opened, the conductance usually becomes larger than  $4e^2/h$ .

### 3.2. The conductance for the antiparallel configuration

Next, we study the antiparallel configuration with  $\theta = \pi$ . The results for the conductance  $G$  are shown in figure 3. One of the main characteristics is a zero conductance when  $E_F$  is near Dirac point (i.e.  $E_F = 0$ ). This is very different from the parallel configuration, in which  $G$  is always larger than  $e^2/h$ . Let us analyze the



conductance in details in the following. Because of  $G(-E_F) = G(E_F)$ , we only discuss the case  $E_F > 0$ . (i) For  $0 < M < \Delta/2$ , the conductance  $G$  is exactly zero in the range  $E_F \in (0, M)$  and becomes  $2e^2/h$  when  $E_F \in (M, M + \Delta)$ . (ii) For  $\Delta/2 < M < \Delta$ ,  $G = 0$  when  $E_F \in (0, \Delta - M)$ , while  $G$  is between 0 and  $2e^2/h$  when  $E_F \in (\Delta - M, M)$  and is exactly  $2e^2/h$  when  $E_F \in (M, M + \Delta)$ . (iii) If  $M$  increases sequentially ( $M > \Delta$ ), around the Dirac point a small salient appears instead of the zero conductance range.

These characteristics of conductance can be well understood from their band structures in figure 4. From the band structures of the antiparallel configuration the spin-up and spin-down electrons contribute equally to the conductance, and we only discuss the spin-up electrons in the following. (i) We discuss the case of  $0 < M < \Delta/2$ , and the corresponding energy band structure is illustrated in figure 4(a). When  $E_F \in (0, M)$ , only the channel  $(0, 0, -1)$  is involved, in which the band is even parity in the left lead and is odd in the right lead. Because of the band-selective rule, its transmission coefficient  $T_{0,0,-1} = 0$ , and  $G = 0$ . On the other hand, when  $E_F \in (M, \Delta + M)$ , the channel  $(0, 0, 0)$  is available so that  $G = 2e^2/h$ . If further increasing  $E_F$ , more channels are opened and the conductance is larger. (ii) We analyze the case of  $\Delta/2 < M < \Delta$ , and the corresponding energy band structure is illustrated in figure 4(b). For  $E_F \in (0, \Delta - M)$ , only the channel  $(0, 0, -1)$  is involved. So  $G = 0$  because of the band-selective rule. When  $E_F \in (\Delta - M, M)$ , the channel  $(1, 0, -1)$  is opened. The parity of the transverse wave function in the center region is different from those in the left and right leads. The incident electrons may be scattered and  $T_{1,0,-1}$  lies between 0 and 1. As a result,  $0 < G < 2e^2/h$ , including the spin-down electrons. By increasing  $E_F$  to the range  $(M, \Delta + M)$ , the channel  $(0, 0, 0)$  is opened, and the total conductance  $G = 2e^2/h$ . Notice that when  $E_F$  is close to but less than  $\Delta + M$ , although the extra channel  $(2, 0, 0)$  is involved, the conductance  $G$  still is  $2e^2/h$  because only the subband 0 is available in the right FM lead.

### 3.3. The magnetoresistance

After obtaining the conductances  $G_P$  and  $G_A$  of parallel and antiparallel configurations, the MR, defined as  $MR = (G_P - G_A)/G_P$ , can be obtained straightforwardly. Figure 5 shows the MR versus the Fermi energy  $E_F$  for different magnetization  $M$ . Here the MR can be very large as far as 100% when  $E_F$  is around the Dirac point. In particular, a plateau with the value 100% is clearly exhibited in the curve of MR- $E_F$ . This 100% MR plateau originates from the zero conductance in antiparallel configuration (see figure 3). It is noticed that the conductance for the parallel configuration is still quite large ( $> e^2/h$ ). This means that the present device not only has the large MR but also has a large variance of the conductance between the parallel and antiparallel configurations. Thus it is a good candidate for the spin valve devices. The width of the 100% MR plateau is determined by magnetization  $M$  and the energy splitting  $\Delta$  between the subbands. When  $0 < M < \Delta/2$ , its width is  $2M$  so it increases with the enhancement of  $M$ . At  $M = \Delta/2$ , the plateau width reaches its widest value  $\Delta$ . By further increasing  $M$ ,

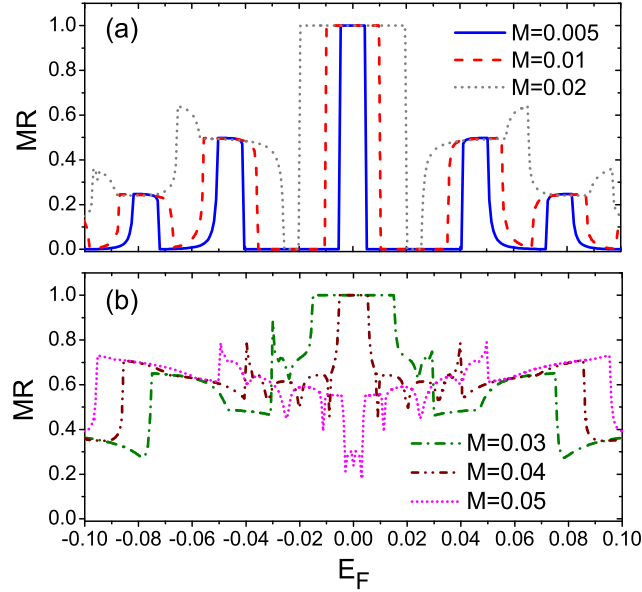


**Figure 5.** (Color online) The MR as a function of  $E_F$  for different magnetization  $M$ . The size of the central region is  $N = 50$  and  $L = 10$ .

the plateau width becomes narrow and it is equal to  $2(\Delta - M)$  when  $\Delta/2 < M < \Delta$ . At  $M = \Delta$ , the 100% MR plateau disappears. When  $M > \Delta$  a valley instead of the plateau appears in the vicinity of  $E_F = 0$ . Therefore for a larger  $\Delta$ , it is more favorable for the formation of the 100% MR plateau. In experiment, the graphene nanoribbon with its width of several-ten or sub-ten nanometers has been fabricated [24]. Taking a  $20\text{nm}$ -width ribbon for an example, its  $\Delta$  is about  $0.12\text{eV}$ , which is usually much larger than  $M$ . In addition, when  $E_F$  deviates far from 0 (i.e. the region of the 100% plateau), the MR may be quite small (see figure 5). This implies that the capability of the graphene-base spin valve is optimal when it works near the Dirac point.

We study the influence of the size of the ribbon between two FM leads on the MR. Figure 6(a) (Figure 6(b)) shows the MR as a function of  $E_F$  for different width  $N$  (length  $L$ ) and a fixed  $L$  ( $N$ ). With the increasing of width  $N$ , the separation  $\Delta$  of the transverse subbands decreases monotonously (with  $\Delta \approx 3\pi t/4N$ ) [31]. In the beginning, the 100% MR plateau is not affected until  $\Delta/2 < M$  (see the curve with  $N = 30, 50$ , and  $100$  in figure 6(a)). Then with further increasing  $N$ , the 100% MR plateau becomes narrow (see the curve with  $N = 150$  in figure 6(a)), and it disappears at the width  $N$  with its  $\Delta = M$ . At last, when the width of ribbon is very wide with its  $\Delta \ll M$ , the MR is very small regardless of other parameters. This result is the same with recent work studying on the infinite wide graphene spin valve device [20]. So it is favorable to select the narrower nanoribbon to fabricate the spin valve. On the other hand, the length change of the central region does not affect the 100% MR plateau at all (see figure 6(b)). Only the shapes of some subplateaus are slightly changed.

In the above discussion, we assumed that the Dirac-point energy  $\epsilon_C$  of the central region is equal to  $\epsilon_\alpha$  of the left and right leads. If  $\epsilon_C$  departs from  $\epsilon_\alpha$ , the conductance

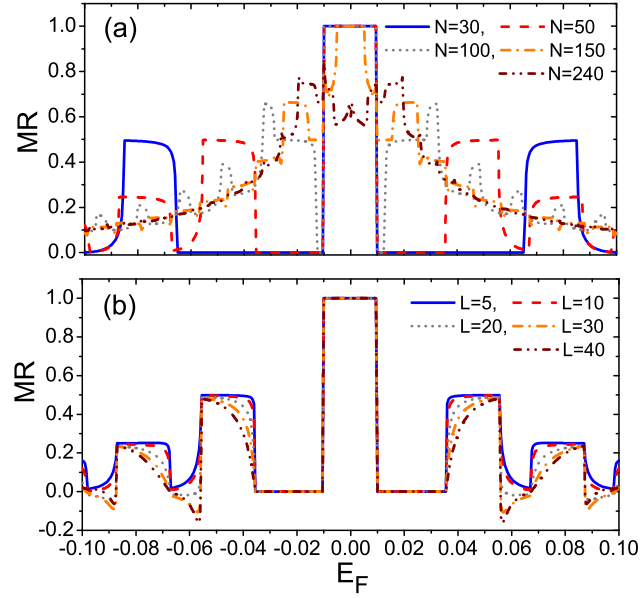


**Figure 6.** (Color online) (a) The MR vs.  $E_F$  for different width  $N$  with the length  $L = 10$  and (b) MR vs.  $E_F$  for different length  $L$  with the width  $N = 50$ . The magnetization  $M = 0.01$ .

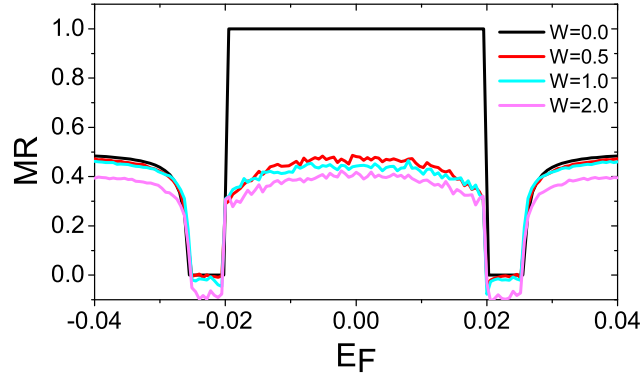


**Figure 7.** (Color online) The MR vs.  $E_F$  for different disorder strength  $W$ . The parameters are  $M = 0.02$ ,  $N = 50$  and  $L = 10$ .

$G$  in the antiparallel configuration still is zero when  $E_F \in (-M, M)$  and  $0 < M < \Delta/2$ , because the parity of transverse wave functions in the left and right FM leads can not match with each other. However, the conductance  $G$  for the parallel configuration is very large ( $> e^2/h$ ). So the 100% MR plateau is not affected by  $\epsilon_C$  slightly departing from  $\epsilon_\alpha$ .

How is the 100% MR plateau affected by the disorder? Here, we consider the Anderson disorder which exists only in the central graphene region. The on-site energy  $\epsilon_C$  in the central region Hamiltonian becomes  $\epsilon_C + w_i$ , where  $w_i$  is uniformly distributed in the range of  $[-W/2, W/2]$ . Figure 7 shows the MR vs.  $E_F$  at different disorder strength  $W$ , in which every MR curve for  $W \neq 0$  is averaged over up to 1000 random

configurations. The MR is reduced by the disorder, but the plateau shape is still hold and the value is about 40%-50% even in quite strong disorder strength.

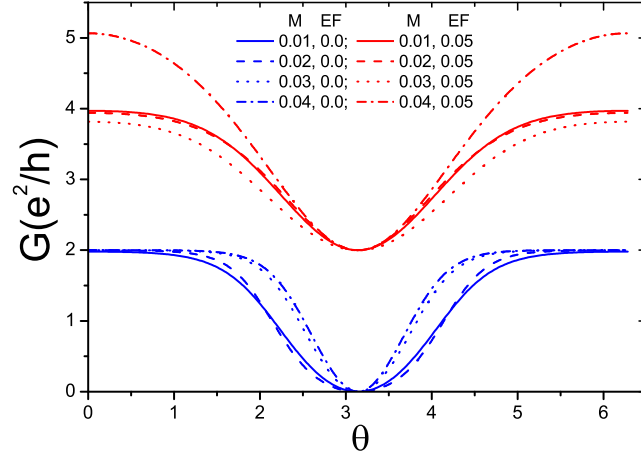


**Figure 8.** (Color online) The conductance  $G$  vs. the angle  $\theta$  for different magnetization  $M$  and different Fermi energy  $E_F$ . The size of the central region is  $N = 50$  and  $L = 10$ .

### 3.4. The conductance for the arbitrary angle $\theta$ of the left and right magnetizations

Now we analyze  $\theta$  dependence of the conductance. In figure 8, the conductance  $G$  as a function of the angle  $\theta$  are plotted with combination of  $M$  and  $E_F$ . Here the shape of the curves  $G$ - $\theta$  is approximately a cosine function regardless of the parameters  $M$  and  $E_F$ . At  $E_F = 0$  (i.e. at the center of the 100% MR plateau), the change quantity of the conductance  $G$  for the angle  $\theta$  from 0 to  $\pi$  is about  $2e^2/h$ , which is quite large. About at  $\theta = 2$ , the derivative  $dG/d\theta$  reaches the extreme value, but at the region of  $0 < \theta < 1$ , the derivative  $dG/d\theta$  is quite small. On the other hand, when  $E_F$  deviates away from the 100% MR plateau, the variation of the conductance  $G$  is also about  $2e^2/h$  or even larger for some values of  $E_F$  (see the curves for  $E_F = 0.05$  in Fig.8), although the MR is about 50% there. However, at the region of  $MR = 0$ , the conductance  $G$  is independent of the angle  $\theta$  (not shown here).

## 4. The case of armchair edge

In this section, we investigate the MR in the armchair edge FM/normal/FM junction. In the case of the armchair edge, there are two types of energy band structure [25]. If the number of transverse atomic layers  $N$  is equal to  $3m$  or  $3m + 1$  ( $m$  is an integer), an energy gap appears. This gap can be quite large for a narrow graphene nanoribbon. When the Fermi energy  $E_F$  is in the gap, the conductance is always very small regardless of the parallel or antiparallel configurations. So it is not interesting even if its MR is very large. For  $N = 3m + 2$ , the graphene nano-ribbon is metallic and its conductance is large.

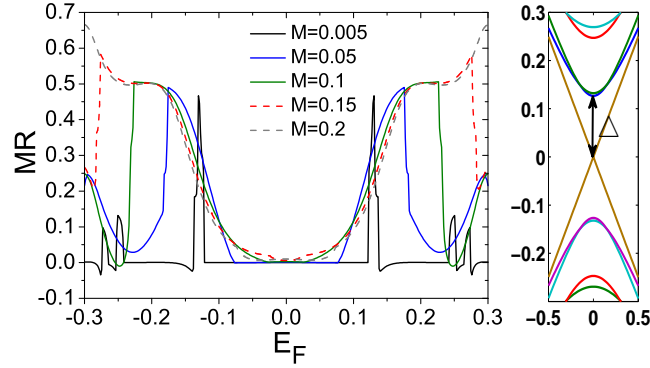


**Figure 9.** (Color online) **Left panel:** The MR as a function of  $E_F$  in the case of the armchair edge with the width  $N = 41$  and the length  $L = 40$  atomic layers in the central region. **Right panel:** The energy band structure of an ideal armchair edge graphene ribbon with the width  $N = 41$ .

Figure 9 shows the MR as a function of Fermi energy  $E_F$  for the metallic armchair edge FM/graphene/FM junction with  $\Delta \approx 0.13t$  for  $N = 41$ . The conductance approaches  $2e^2/h$  for both the parallel and antiparallel configurations at a large range of  $E_F$  around zero energy. As a result the MR is very small regardless of  $M > \Delta$  and  $M < \Delta$ . On the other hand, when  $E_F$  is far away from 0 (e.g.  $E_F > \Delta$ ), the MR can be over 50% in some regions of  $E_F$ . Anyway, the property of MR of the zigzag edge ribbon is much better than that of the armchair edge ribbon. So it is more favorable to fabricate the spin valve devices by using the zigzag edge ribbon. In experiment, the graphene nanoribbon with the specific parity edge has already been successfully fabricated [24].

## 5. Conclusions

In summary, we have studied the electronic transport and magnetoresistance (MR) in graphene-based ferromagnetic/normal/ferromagnetic junction where the finite width and the arbitrarily relative orientation between the lead magnetizations are taken into account. For the zigzag edge case, the conductance for the parallel configuration is always larger than  $e^2/h$  under any parameter condition, but for the antiparallel configuration the conductance is exactly zero when Fermi energy is around the Dirac point due to the band-selective rule. This leads to a 100% MR plateau. The 100% MR plateau is almost not affected by the length of the central graphene region. With the increasing of the width of the ribbon, the 100% MR plateau is kept stable in the beginning, but is smeared at the wide ribbon limit. In the presence of the disorder, the MR is slightly suppressed, but can still keep the plateau shape with the value about 50% even in quite large disorder strengths. When the orientation between magnetizations of two ferromagnetic leads is arbitrary, the conductance versus the relative angle  $\theta$  is similar to a cosine formation. What's more, for the armchair edge case, the MR is relatively small. Therefore, it is more favorable to fabricate the graphene-based spin valve devices by using the zigzag edge graphene ribbons.

## Acknowledgments

We gratefully acknowledge the financial support from NSF-China under Grants Nos. 10525418, 10734110, and 10821403, the 973 Program Project No. 2009CB929103, and the Research Grant Council of Hong Kong under Grant No. HKU 7042/06P and HKU 10/CRF/08. Shu-guang Cheng was supported by the Science Foundation of Northwest University (No.09NW29).

## References

- [1] Geim A K and Novoselov K S 2007 *Nature Materials* **6** 183
- [2] Semenoff G W 1984 *Phys. Rev. Lett.* **53** 2449
- [3] Novoselov K S, Geim A K, Morozov S V, Jiang D, Katsnelson M I, Grigorieva I V, Dubonos S V and A. A. Firsov 2005 *Nature* **438** 197
- [4] Williams J R, DiCarlo L and Marcus C M 2007 *Science* **317** 638
- [5] Novoselov K S, Geim A K, Morozov S V, Jiang D, Zhang Y, Dubonos S V, Grigorieva I V and Firsov A A 2004 *Science* **306** 666; Bolotin K I, Sikes K J, Jiang Z, Fudenberg G, Hone J, Kim P and Stormer H L 2008 *Solid State Communications* **146** 351
- [6] Tombros N, Jozsa C, Popinciuc M, Jonkman H T and Van Wees B J 2007 *Nature (London)* **448** 571
- [7] Kane C L and Mele E J 2005 *Phys. Rev. Lett.* **95** 226801
- [8] Yazyev O V 2008 *Nano Lett.* **8** 1011
- [9] Prinz C A 1998 *Science* **282** 1660; Wolf S A, Awschalom D D, Buhrman R A, Daughton J M, von Molnár S, Roukes M L, Chtchelkanova A Y and Treger D M 2001 *Science* **294** 1488
- [10] Haugen H, Huertas-Hernando D and Brataas A 2008 *Phys. Rev. B* **77** 115406
- [11] Son Y -W, Cohen M L and Louie S G 2006 *Nature* **444** 347
- [12] Lin H -H, Hikihara T, Jeng H -T, Huang B -L, Mou C -Y and Hu X 2009 *Phys. Rev. B* **79** 035405
- [13] Hill E W, Geim A K, Novoselov K, Schedin F and Blake P 2006 *IEEE Trans. Magn.* **42** 2694
- [14] Józsa C, Popinciuc M, Tombros N, Jonkman H T and van Wees B J *Phys. Rev. B* **79** 081402
- [15] Han W, Wang W H, Pi K, McCreary K M, Bao W, Li Y, Miao F, Lau C N and Kawakami R K 2009 *Phys. Rev. Lett.* **102** 137205
- [16] Žutić I, Fabian J and Das Sarma S 2004 *Rev. Mod. Phys.* **76** 323
- [17] Saffarzadeh A and Asl M G 2009 *Eur. Phys. J. B* **67** 239
- [18] Muñoz-Rojas F, Fernández-Rossier J and Palacios J J *Phys. Rev. Lett.* **102** 136810
- [19] Bai C and Zhang X 2008 *Phys. Lett. A* **372** 725
- [20] Brey L and Fertig H A 2007 *Phys. Rev. B* **76** 205435
- [21] Ding K -H, Zhu Z -G and Berakdar J 2009 *Phys. Rev. B* **79** 045405
- [22] Kim W Y and Kim K S 2008 *Nature Nanotechnology* **3** 408
- [23] Stauber T, Castro E V, Silva N A P and Peres N M R 2008 *J. Phys.: Condens. Matter* **20** 335207; Wu Q -S, Zhang S -Z and Yang S -J 2008 *J. Phys.: Condens. Matter* **20** 485210; Zhang Z -Y 2009 *J. Phys.: Condens. Matter* **21** 095302
- [24] Li X, Wang X, Zhang L, Lee S and Dai H 2008 *Science* **319** 1229
- [25] Cresti A, Nemeč N, Biel B, Niebler G, Triozon F, Cuniberti G and Roche S 2008 *Nano Res* **1** 361
- [26] Saito R, Dresselhaus G and Dresselhaus M S 1998 *Physical Properties of Carbon Nanotubes* (Imperial College Press, London)
- [27] Datta S 1995 *Electronic transport in Mesoscopic Systems* (Cambridge University Press, Cambridge)
- [28] Lee D H and Joannopoulos J D 1981 *Phys. Rev. B* **23** 4997
- [29] Sancho M P L, Sancho J M L, and Rubio J 1985 *J. Phys. F: Met. Phys.* **15** 851
- [30] Nakabayashi J, Yamamoto D, and Kurihara S 2009 *Phys. Rev. Lett.* **102** 066803

- [31] Cresti A, Grosso G, and Parravicini G P 2008 *Phys. Rev. B* **77** 115408